HHS Public Access

Author manuscript

NMR Biomed. Author manuscript; available in PMC 2017 March 01.

Published in final edited form as:

NMR Biomed. 2016 March ; 29(3): 256–263. doi:10.1002/nbm.3455.

Repeatability of ^{31}P MR spectroscopic imaging in the human brain at 7 T with and without the Nuclear Overhauser Effect

Miriam W. Lagemaat[1], **Bart L. van de Bank**[1], **Pascal Sati**[2], **Shizhe Li**[3], **Marnix C. Maas**[1], and **Tom W.J. Scheenen**[1,2,4]

[1]Department of Radiology and Nuclear Medicine, Radboud University Medical Center, Nijmegen, the Netherlands [2]Laboratory of Functional and Molecular Imaging, National Institute of Neurologiocal Disorders and Stroke, National Institutes of Health, Bethesda MD, USA [3]MRS Core Facility, National Institute of Mental Health, National Institutes of Health, Bethesda MD, USA [4]Erwin L. Hahn Institute for Magnetic Resonance Imaging, University Duisburg-Essen, Essen, Germany

Abstract

An often employed strategy to enhance signals in ^{31}P MR spectroscopy is the generation of the nuclear Overhauser effect (NOE) by saturating the water resonance. However, NOE allegedly increases the variability of the ^{31}P data, because variation is reported in NOE enhancements. This would negate the SNR gain it generates. We hypothesized that variation in NOE enhancement values is not due to variability in the NOE itself, but that it is attributable to measurement uncertainties in the values used to calculate the enhancement. If true, the expected increase in SNR with NOE would improve the repeatability of ^{31}P MR spectroscopy measurements. To verify this hypothesis, a repeatability study of native and NOE-enhanced ^{31}P MRSI was performed in the brain of 7 healthy volunteers at 7T.

The repeatability coefficient (RC) and the coefficient of variation in repeated measurements (CoV_{repeat}) were determined per method, and the 95% limits of agreement (LoA) between native and NOE-enhanced signals were calculated. The variation between the methods, defined by the LoA, is at least as great as that predicted by the RC of each method. The sources of variation in NOE enhancements were determined using variance component analysis.

In the 7 metabolites with a positive NOE enhancement (9 metabolite resonances assessed), CoV_{repeat} improved on average by 15%. The LoAs could be explained by the RCs of the individual methods for the majority of the metabolites, generally confirming our hypothesis. Variation in NOE enhancement was mainly attributable to the factor repeat, but between-voxel effects were also present for phoshpoethanolamine and (glycero)phosphocholine. CoV_{repeat} and fitting error were strongly correlated and improved with positive NOE.

Our findings generally indicate that NOE enhances the signal of the metabolites, improving the repeatability of metabolite measurements. Additional variability due to NOE was minimal. These findings encourage the use of NOE-enhanced ^{31}P MRSI.

Keywords

repeatability; reproducibility; 7 Tesla; ultra-high field; MR spectroscopy

Introduction

Phosphorus (^{31}P) MR spectroscopy is a non-invasive technique to study tissue metabolism under various physiological and pathophysiological conditions. Human organs and tissues frequently investigated using ^{31}P MRS include the liver (1,2), skeletal muscle (3,4), the heart (5) and the brain (6,7), and studies concerning the prostate (8), the placenta (9), and breast (10) have also been reported recently. Metabolic changes can be followed over time with dynamic ^{31}P MRS, and MR spectroscopic imaging (MRSI) allows the two- or three-dimensional mapping of metabolites to study their spatial distribution.

The low intrinsic sensitivity of in vivo ^{31}P MRS and MRSI however impedes the regular use of these techniques. Obviously, advances in radiofrequency (RF) coil design and increases in magnetic field strength have been embraced to gain ^{31}P sensitivity enabling reduced overall acquisition times or increased spatial resolution. Sensitivity of ^{31}P spectra can also be improved by adding proton (^{1}H) irradiation to the MR sequence (11–13). Proton irradiation may activate two physical mechanisms: decoupling and the nuclear Overhauser effect (NOE).

The first process, proton decoupling, is particularly useful at clinical field strengths (1.5-3 T), where the line width of the resonances of interest after shimming can be of similar size as the weak heteronuclear ^{31}P-^{1}H J-couplings (5-7 Hz). Without proton decoupling the coupled metabolites split into doublets or triplets, giving rise to broad resonances and spectral overlap. Many metabolites present in an in vivo ^{31}P spectrum contain one or more weak ^{31}P-^{1}H J-couplings, i.e. phosphoethanolamine (PE), phosphocholine (PC), glycerophosphoethanolamine (GPE), glycerophosphocholine (GPC), 2,3-diphosphoglycerate, α-adenosine triphosphate (αATP) and nicotinamide adenine dinucleotide (NAD^+ and NADH). The improvement in spectral resolution obtained by decoupling reduces the spectral overlap of the ^{31}P metabolites and thus allows better peak assignment and consequently better spectral quantification. Decoupling can be achieved by applying high-power broadband proton irradiation during ^{31}P signal acquisition, creating high specific absorption rates (SAR) at higher field strengths.

The second process of signal improvement, the NOE, uses low-power proton irradiation to saturate the water resonance in between ^{31}P signal acquisitions. The saturated water protons can increase the steady state magnetization of the ^{31}P nuclei through dipolar interactions, resulting in enhanced ^{31}P metabolite signal intensities. In vivo enhancements up to 80% have been reported (14), which encourages the use of NOE-enhanced ^{31}P MRS or MRSI. Because NOE requires considerably less power than decoupling, it is also suited for higher magnetic field strengths.

Absolute NOE enhancement values depend on the extent to which the dipolar ^{31}P-^{1}H interaction mediates T_1 relaxation of the ^{31}P spins (15). The enhancement values therefore

vary between metabolites, and are dependent on the mobility of the metabolites in the tissue and magnetic field strength (14,16–22). Sufficient saturation of the water resonance is essential to maximize the NOE enhancement (12,13), and needs to be optimized for each sequence. At ultrahigh magnetic field strengths it is even more important to determine the minimum transmit RF amplitude (B_1^+) for constant NOE, because of the known spatial inhomogeneities in the B_1^+ field (22).

The in vivo NOE signal enhancement indeed seemed very beneficial initially (14), but considerable variation was later reported in NOE enhancement values per metabolite, even if the measurements were calibrated well (19,20,22). This has raised concerns that using NOE might add variability to the ^{31}P data, negating the gain in signal-to-noise ratio (SNR). We hypothesized that variation in NOE enhancement values is not due to variability in the NOE itself (i.e. non-constant NOE enhancements because of natural variation or inadequate NOE calibration), but that it is attributable to measurement uncertainties in the values used to calculate the NOE enhancement. If true, this would argue for the use of NOE as the SNR is expected to increase, which would potentially decrease measurement uncertainties. To test this hypothesis repeated measurements with both methods, i.e. native, non-enhanced ^{31}P MRS/ MRSI and NOE-enhanced MRS/ MRSI are needed. The measurement uncertainties of the two methods, estimated by their repeatabilities, limit the amount of agreement possible between the two methods, and thus define a minimum variation in NOE enhancement values per metabolite (23).

Ultimately, one wishes to answer the question whether or not to use NOE in ^{31}P MRS/MRSI studies in any tissue at any field strength. Because of the dependency of NOE enhancements on dipolar relaxation processes and saturation efficiency, spatial variations in NOE enhancement might be possible, and these may depend on the tissue type and state (healthy and diseased) and the field strength. To reduce complexity regarding all these issues, the research question in this study was narrowed down to the possible beneficial effect of NOE on ^{31}P MRSI of the healthy human brain at 7 T. To answer this question we performed repeated measurements of native ^{31}P MRSI and NOE-enhanced ^{31}P MRSI in the brain of healthy volunteers at 7 T.

Experimental

Hardware

Measurements were performed on a 7 T whole-body MR research system (MAGNETOM, Siemens Healthcare, Erlangen, Germany). An eight-rung high?pass quadrature birdcage coil tuned to ^{31}P (120.3 MHz) was used (24), which was designed to fit within a homebuilt eight-channel ^{1}H array head coil with meander elements (25). The safety of the coil combination was assessed previously (24). ^{1}H MR imaging and ^{1}H saturation for NOE generation was performed with an add-on system for RF shimming, which also performed real-time SAR monitoring on both the ^{1}H and the ^{31}P channels (26,27).

Subjects

Seven healthy volunteers (6 male, 1 female, mean age 30 years, range 21-39 years) participated in this study. The study was conducted in accordance with all guidelines set forth by the approving institutional review board, and signed informed consent was obtained from all subjects before the measurements.

NOE generation

To ensure efficient water saturation for NOE, a wideband alternating-phase low-power technique for zero residual splitting (WALTZ-4, historically used for decoupling) (28) was adopted. The WALTZ-4 train was applied during the full TR, except during the ^{31}P RF pulse and the 204 ms of signal acquisition. The durations of the individual pulses of one WALTZ sub-train were 2.5, 5.0 and 7.5 ms, with 2.5 ms pauses in between segments, requiring 14 WALTZ-4 trains of 90 ms each per repetition time. The minimum power needed to generate constant NOE enhancements for this setting of WALTZ-4 was determined to be 30 Hz in previous phantom experiments (partly presented in (22)).

MR measurement protocol

Anatomical images for planning of the 3D ^{31}P MRSI measurements were acquired using a magnetization prepared 3D T1-weighted gradient echo (MPRAGE) sequence. Magnetic field (B_0) phasemap shimming was performed to optimize the B_0 homogeneity in the posterior region of the brain. ^{1}H transmit RF amplitude (B_1^+) was maximized in the same region using RF shimming. The amplitude of WALTZ-4 pulses to generate a constant NOE was set to reach at least 30 Hz in the posterior part of the brain by using absolute B_1^+ maps (fig. 1a). These maps were acquired using a magnetization prepared gradient echo sequence (TR = 5000 ms, TE = 5 ms, magnetization preparation flip = 90°, excitation flip angle = 10°) (29).

Flip angle calibration for ^{31}P was performed using a slice selective pulse acquire sequence (6 ms excitation pulse, TR = 15 s), selecting a 40 mm thick slice through the posterior brain (fig. 1b). The amplitude of the RF pulse was varied between shots to find the maximum magnitude of the phosphocreatine (PCr) peak. This maximum was assumed to correspond to 90° excitation, and all ^{31}P RF amplitudes in the subsequent MRSI sequences were scaled relative to this value.

For the 3D ^{31}P MRSI measurements, a pulse acquire sequence was used with a 300 μs block pulse for excitation (flip angle = 45°) and a TR of 1500 ms. The field of view (FOV) was set to 240 × 240 × 240 mm and the 3D phase encoding matrix to 12 × 12 × 8, creating isotropic dimensions in the transverse plane. The delay between the excitation pulse and the start of data acquisition was 410μs. An elliptical k-space acquisition scheme was applied (1 average) and k-space was Hamming filtered (100%). The nominal voxel size of 20 × 20 × 30 mm is therefore enlarged to a ellipsoid-shaped voxel volume of approximately 38 cm^3 (30). The MRSI acquisition of 7 min 48 s was repeated four consecutive times. The first and third MRSI acquisitions were obtained without ^{1}H irradiation (native), the second and the fourth with ^{1}H irradiation to generate the NOE.

Data analysis – voxel selection and spectral fitting

Three non-neighboring MRSI voxels were selected per volunteer (fig. 1c). Care was taken to select only voxels that received a minimum ^{1}H B_1^+ of 30 Hz in the case of NOE generation, that were situated completely within the brain, and that showed good spectral quality in all four MRSI datasets. Different voxel locations were chosen per volunteer. The average B_1^+ in each selected voxel was estimated using the absolute B_1^+ map.

The ^{31}P spectra of the selected voxels were fitted with Metabolite Report, a work in progress package from Siemens Healthcare (Erlangen, Germany). Metabolite Report performs automated, prior knowledge based, complex fitting in the time domain and has previously been applied to 7 T ^{31}P spectroscopy data of the prostate (8). The spectral resonances PE, PC, GPE, GPC, inorganic phosphate (Pi), α-, γ-, β-ATP and NAD^+/ NADH were fitted using Gaussian lineshapes, while PCr was fitted with a Lorentzian lineshape. Prior knowledge of the relative peak frequencies and the ^{31}P J-coupling patterns in the ATPs was used. The line widths of PE, PC, GPE, and GPC were assumed to be the same and thus constrained to each other. The quality of the spectral fit was assessed using the Cramér-Rao lower bound (CRLB) values and qualitatively by visual inspection by spectroscopist. The CRLB values of the fits with and without NOE were compared using a paired t-test per metabolite.

Only metabolite fits with a CRLB below 30% were considered reliable. The original spectra and the fitting results were visually inspected, and if a metabolite peak was visually present and its fit was assigned to the correct resonance, giving a minimal residue, the fitting result was accepted. Only metabolites which passed both quality checks were used in further analyses.

The NOE enhancement (η) per metabolite in each selected voxel was calculated by

$$\eta = \frac{\overline{NOEenh}_{repeat} - \overline{native}_{repeat}}{\overline{native}_{repeat}}, \quad (1)$$

with $\overline{NOEenh}_{repeat}$ and $\overline{native}_{repeat}$ representing the mean metabolite peak integral of the two repeated measurements using NOE-enhanced and native MRSI respectively.

Theory of repeatability and method comparison

To be able to answer our research question, we used an approach presented by Bland and Altman to assess the agreement between two methods of clinical measurement (23). The term “agreement” might be misleading here, since a difference between the native and NOE-enhanced method is expected because of the NOE enhancements for most metabolites. However, the agreement between methods, or the lack of it, has two components: the bias, i.e. the mean difference between the methods, and the random variation. The random variation is at least as great as that predicted by the repeatability of each method, but may be larger because of heterogeneity between individual measurement units (e.g. subjects, but in this study individual voxels as well). For correct interpretation of the measure of agreement between methods it is thus essential to first determine the repeatability of each individual method.

Statistical analyses of repeatability and method comparison

Useful measures for the repeatability of a method are the repeatability coefficient (RC) and the coefficient of variation in repeated measurements (CoV_{repeat}). The RC defines the width of the interval within which we expect the absolute difference between two measurements with the same method to lie in 95% of the cases. It is defined as $\sqrt{2} \cdot 1.96 \cdot \sigma_{repeat} = 2.77 \cdot \sigma_{repeat}$, where σ_{repeat} is the standard deviation of repeated measurements. Once the RCs are known for two methods, their repeatability intervals (2*RC) can be directly compared to the interval of the 95% limits of agreement (LoA) between the two methods (see below), allowing to assess how much of the observed variation between the methods can be explained by the repeatability of the individual methods (23).

In the present work, σ_{repeat} was estimated for each metabolite and each method (native and NOE-enhanced) by decomposing the total observed variance into the factors “between-subject”, “between-voxel” (or “within-subject”), and “repeat” (or “within-voxel”):

$$\sigma^2_{tot} = \sigma^2_{between-subject} + \sigma^2_{between-voxel} + \sigma^2_{repeat} \quad (2)$$

This was done by fitting a 3-level no-predictors linear mixed model to the data of each metabolite and method, in which “subject” and “voxel” were treated as level-3 and level-2 random intercepts, respectively.

The CoV_{repeat} is a normalized measure of σ_{repeat} to study relative repeatability:

$$CoV_{repeat} + \frac{\sigma_{repeat}}{\mu} * 100\% \quad (3)$$

with μ the mean of the metabolite integrals of all voxels and repeated measurements, without or with NOE (μ_{native} *and* μ_{NOEenh}). The native and NOE-enhanced CoV_{repeat} were determined per metabolite and for metabolite ratios, using standard error propagation methods. The apparent CoV_{repeat} of NOE-enhanced metabolite intensities corrected for their enhancement (which would be needed for absolute quantification) was calculated using error propagation as well. A relation between quality of the metabolite fits and the repeatabilities of the metabolites was explored by the Pearson correlation between CRLB and COV_{repeat}.

The agreement between native and NOE-enhanced ^{31}P MRSI was quantified using their 95% limits of agreement (LoA). The interval of 95% LoA is determined by the overall bias between the two methods $\left(\bar{d}\right)$ and the variation around this mean difference, expressed by the standard deviation of the differences (σ_d):

$$95\%\text{LoA} = \bar{d} \pm 1.96 * \sigma_d. \quad (4)$$

The LoA were calculated using $\overline{native}_{repeat}$ and $\overline{NOEenh}_{repeat}$ (the mean integrals of the two repeated measurements per voxel with each method). The overall bias $\bar{d}$ was estimated using

$$\bar{d} = \left\langle \overline{NOEenh}_{repeat} - \overline{native}_{repeat} \right\rangle, \quad (5)$$

where the brackets denote the average over all voxels. Since we include all data in calculating the agreement, using the two repeated measures for $\overline{native}_{repeat}$ and $\overline{NOEenh}_{repeat}$, the observed standard deviation of the differences between pairs of means of repeated measures $s_{\bar{d}}$ needs an adaptation to attain the standard deviation of the differences between the methods σ_d (23):

$$\sigma_2^d = S\frac{2}{d} + \frac{\sigma^2_{repeat\_native}}{2} + \frac{\sigma^2_{repeat\_NOEenh}}{2} \quad (6)$$

The 95% LoA and the repeatability intervals were compared for each metabolite. If these ranges are similar, then the (lack of) agreement is fully explained by the (lack of) repeatability. If the range of the 95% LoA is considerably wider than the repeatability intervals of the individual methods, then (some) additional heterogeneity exists between the individual voxels and subjects in NOE enhancement (i.e. NOE would introduce additional signal variation).

The presence of NOE-induced additional signal variation between voxels and subjects was also assessed by variance components analysis of measured NOE enhancements, using the same model as described above (Eq. 2).

The effect of NOE on the peak integrals of individual metabolites was tested for significance using similar 3-level mixed models as above, with “NOE” as an additional fixed factor. To test whether the minimum ^{1}H power criterion of 30 Hz for constant NOE was sufficient in vivo, linear mixed models of the NOE enhancements of the individual metabolites were constructed, which included local B_1^+ as a fixed covariate. The possible effect of local B_1^+ on NOE enhancement was assessed using these models. Statistical test outcomes with p-values < 0.05 were considered significant.

Results

All subjects completed the full scan protocol, without having to repeat any measurements. The minimum power condition of 30 Hz for NOE was reached in every subject in the posterior part of the brain (example in figure 1). All measurements could be performed within the simulation-based SAR limits (15W/6 min into the coil), governed by local SAR limits and an additional 40% safety margin. The power on the ^{1}H channel had the highest contribution to the total SAR. High quality spectra were obtained throughout large parts of the brain, but to meet the 30 Hz criterion on ^{1}H, only voxels from the posterior brain region were selected for quantification. The βATP intensity was strongly attenuated or not present because it was outside the effective bandwidth of the excitation pulse and it was therefore excluded from further analysis. The PC and NAD resonances were sometimes only visible as a small shoulder on the right side of respectively PE or αATP. An example of a spectral fit is presented in the supplementary material.

Small variations in spectral patterns between repeated measurements using the same method were observed, and NOE enhancements could also be observed visually (fig. 2). For all metabolites except αATP the quality of the spectral fit was significantly better in the NOE-enhanced ^{31}P MRSI data than in the native ^{31}P MRSI data (table 1). From 378 metabolite signals (7 volunteers * 2 measurements * 3 voxels * 9 signals) in the native ^{31}P MRSI data, 15 metabolite fits had a CRLB above 30% (PC: 2, NAD: 13), while from 378 signals in the NOE-enhanced ^{31}P MRSI data, this occurred 2 times (PC: 1, NAD: 1). None of the metabolite signals with a CRLB below 30% was discarded by visual inspection.

NOE enhancement factors varied between metabolites (table 1, fig. 3), with mean enhancements up to 39%. The fitted ^{31}P metabolite integrals were significantly higher ($p \leq 0.003$) using NOE for all metabolites except αATP. PE, PC, Pi, GPE, GPC and NAD showed considerable variation in NOE enhancement between the voxels, but outliers did not result from the same voxels.

The repeatability coefficients of native and NOE-enhanced ^{31}P MRSI were comparable for all metabolites except for GPE and NAD (fig. 4a). GPE was considerably less repeatable with NOE, whereas NAD was better repeatable with NOE. Because of the signal increase with NOE, the CoV_{repeat} (relative repeatability within voxels) was better in the NOE-enhanced data for PE, PC, Pi, GPC, PCr, and NAD (table 2, fig. 4b). Similarly, the relative repeatability of metabolite ratios containing these metabolites improved with NOE (table 2). In general, CoV_{repeat} was best for PCr, γATP and αATP, i.e. metabolites with the highest signal integrals and smallest fitting errors (table 2). Correcting NOE-enhanced metabolite intensities for their enhancement factors for absolute quantification purposes causes larger variation in all metabolites compared to the native or NOE-enhanced data (table 2). A strong correlation existed between mean CRLB and COV_{repeat} (R^2=0.91, $p<0.0001$, fig. 5).

The agreement between native and NOE-enhanced ^{31}P MRSI, expressed by the 95% LoA, was in the range of the repeatability intervals of the individual methods for all metabolites except PE (fig. 4a). The variation in NOE enhancements between subjects was dominated by the "repeat" component for all metabolites (mean 85%, minimum 60% of total variance for PE, fig. 4b). Between-subjects variations were negligible (mean 3%, maximum 10% of total variance), while between-voxel differences explained a noticeable fraction of the variance only for PE (40%), GPC (34%) and PC (19%). Absolute ^{1}H B_1^+ (≥30 Hz) was not a significant predictor for NOE enhancement levels ($p>0.11$) for any of the metabolites except PC ($p=0.04$). For the latter, ^{1}H B_1^+ only partially explained the between-voxel variations: controlling for this factor still yielded unexplained between-voxel variations of 10% of the total variation.

Discussion

This study was performed to answer the question "should we use NOE in ^{31}P MRS(I) or not?". To a great extent, this question can be answered with yes, but we will discuss several aspects which should be taken into consideration in deciding upon using NOE or not.

Significantly higher ^{31}P signals were measured using NOE for most metabolites, while none of the metabolites showed a (significant) decrease in signal. Moreover, the signal enhancement significantly improved fitting quality of the metabolite resonances with a positive NOE enhancement. These favorable aspects of NOE at 7T have been reported before (19,22) and especially the first reason has historically led to the use of NOE in in vivo studies. However, when quantifying NOE enhancements per metabolite by using native and NOE-enhanced ^{31}P MRSI data, considerable variation in enhancement values was observed in this study, reproducing findings in many previous studies of different tissues at different field strengths (16–19,21,22). This variation may indicate lack of agreement between both methods, and in unreplicated studies this can be interpreted as NOE adding variability to the data. However, it might also be caused by poor repeatability of (one of) the methods. The design of this study allowed us to put this variation into the perspective of the repeatability of the individual methods. For a good repeatability study, all measurements need to be performed with the same system and method, within a short period of time. This is in contrast to reproducibility studies, in which the variation in measurements is observed under changing conditions (31). Our hypothesis was that variation in NOE enhancement values is caused by the limited repeatability of the underlying methods (native and NOE-enhanced ^{31}P MRSI). The measurement uncertainties of the ^{31}P metabolite values will propagate in the calculation of the NOE enhancement.

The similarity of the 95% LoA of both methods and the 95% repeatability intervals of each method as well as the dominance of the factor repeat in the NOE enhancement confirmed our hypothesis. The metabolites PC, Pi, GPE, GPC and NAD showed considerable variation in NOE enhancements, but this apparent lack of agreement between the methods could be traced back to the repeatabilities of both methods for these metabolites. It depends upon the application of the method what relative repeatability can be considered sufficient, but for all these metabolites the CoV_{repeat} was above 10% with native ^{31}P MRSI, and improved for all but GPE with NOE. Similarly, the CoV_{repeat} of ratios containing these metabolites improved with NOE. GPE showed both a higher absolute and relative repeatability with NOE, although a NOE enhancement of 30.1% was observed. We suspect this finding to be incidental, resulting from the limited sample size and low SNR of this metabolite. NOE enhancements are known to be dependent on dipolar relaxation time (15), which might be affected by pH or temperature, but all circumstances were kept the same between the repeated measurements, so it is unlikely that the dipolar relaxation time has changed within a voxel between the two repeated NOE-enhanced ^{31}P MRSI measurements. The relative repeatability of metabolites with endogenously higher signal intensities and smaller fitting errors was better (PCr, γATP and αATP) compared to the metabolites with lower signal intensities, even though their absolute repeatability was slightly worse. These metabolites also showed the smallest variation in their NOE enhancement values. The strong linear correlation between quality of fit, expressed by the CRLB, and the relative repeatability indicated that CRLB values present a good measure of relative repeatability of ^{31}P MRSI.

PE, and to a smaller extent PC and GPC, showed an improvement in relative repeatability with NOE, but both the Bland-Altman based analysis and the decomposition of variance in NOE enhancements indicated the presence of additional heterogeneity between voxels next to repeatability variations. We tested and excluded local ^{1}H B_1^+ to be the reason for

additional variation with NOE. A different reason for additional variation between voxels with NOE could be spatial differences in dipolar interaction between the ^{1}H and ^{31}P spins related to tissue type. Because of the large true voxel size in this study, selected voxels contained a mixture of gray and white matter, and they were sometimes also contaminated with skull tissue or cerebral fluid. The diffuse border of the voxels (30,32) precluded analysis of the exact tissue distribution within the spectroscopic voxels by segmentation. To study the possible effect of tissue type on NOE enhancements would require a much higher spatial resolution and thus considerably longer acquisition times.

The effect of proton decoupling on the repeatability of ^{31}P MRSI, solely or in combination with NOE, was not investigated in this study. The beneficial effect of proton decoupling decreases with field strength, and it adds considerably to the SAR burden. In this 7 T study we opted to saturate the water resonance to generate the NOE with a strategy well-known from decoupling; the WALTZ-4 irradiation scheme. This irradiation scheme provides a relatively broadband saturation, which reduces the sensitivity of water saturation to local B_0 inhomogeneities. At clinical field strengths one could also use continuous wave irradiation to saturate the water resonance. Since the power needed for water saturation with WALTZ-4 contributed significantly to the SAR in our study, it would be of interest to determine if a lower ^{1}H B_1^+ would be sufficient for in vivo experiments compared to phantom experiments.

In the current study, we homogenized B_0 and ^{1}H B_1^+ in the posterior part of the brain only, whereas for clinical studies homogenization over the whole brain is probably more often required. At clinical field strengths the ^{1}H B_1^+ and B_0 distributions are intrinsically more homogeneous than at 7 T, facilitating this prerequisite. Other coil configurations or parallel transmit techniques combined with tailored RF pulses may also increase the size of the ^{1}H region that can be excited homogeneously at 7 T (33). Automatic scanner adjustments of clinical MR scanners obviate the need to calibrate the ^{1}H pulse amplitudes for NOE, which was a relative time-consuming procedure in this study. The minimum ^{1}H B_1^+ for constant NOE using a specific saturation strategy should however be determined in a pre-study. In cases where non-uniformities in the ^{1}H RF field are expected, e.g. when using ^{1}H surface coils or at ultra-high field strengths, careful examination of the field distribution and amplitude is needed before employing NOE. The necessity of ^{31}P flip angle calibration in every single subject has to be assessed in a larger cohort. In the 7 subjects within this study, the ^{31}P B_1^+ was very similar. It is very common to use a pre-determined, constant B_1^+ for multinuclear experiments at clinical field strengths, or a pre-determined fixed multiplication factor between the X-nucleus and the automated ^{1}H B_1^+ calibration, because of the lack of automated procedures for multinuclear coils.

The results of this ^{31}P MRSI study in the brain at 7T can guide human ^{31}P MRS(I) investigations of the brain and of other tissues including those performed at different field strengths. The improvement of relative repeatability of ^{31}P metabolites with positive NOE enhancements allows detection of smaller differences in metabolite intensities or ratios. This is of interest in follow-up studies or in the comparison of groups (e.g. healthy vs. patient). NOE-enhanced metabolite ratios obviously differ from native ratios, but they are more repeatable. When reporting NOE-enhanced metabolite ratios, it is of importance to clearly

describe the way NOE is generated. This allows others to perform similar experiments, thus enabling between-site comparisons. When absolute quantification of ^{31}P metabolite concentrations is preferred, it has to be realized that data should be corrected for the NOE enhancement, which introduces an additional source of variation to the quantification. Although it is known that NOE enhancements can vary between tissues (14,16–22), it remains uncertain if variations within an organ can exist as well. As discussed above we found an indication that this might be the case for NOE enhancements of PE, PC and GPC. It is similarly unknown if NOE is different in diseased tissue compared to normal tissue or during activation (exercise), or if there are changes in NOE with age. In diseased tissue, T_1 relaxation times of ^{31}P may change (34), which may have an effect on the absolute NOE enhancements. A larger repeatability study with a more heterogeneous study population, including patients, would be needed to confirm if the above-mentioned possible differences in NOE can be distinguished from the measurement uncertainties of native and NOE-enhanced ^{31}P MRSI. It would also be of interest to study reproducibility of NOE enhanced ^{31}P MR data by measuring subjects on different days (20,35). This allows calculation of sample sizes needed to reveal significant differences in certain metabolite ratios for paired (e.g. response to therapy) and independent (e.g. patient vs. control) studies.

In conclusion, the signal enhancement generated by NOE improved relative repeatability of brain ^{31}P MRSI in healthy volunteers. Variations in NOE enhancements per metabolite could almost completely be explained by the repeatability of native and NOE-enhanced ^{31}P MRSI. For these reasons, the use of NOE-enhanced ^{31}P MRSI is encouraged.

Supplementary Material

Refer to Web version on PubMed Central for supplementary material.

Acknowledgement

We thank Arend Heerschap for constructive comments and Elisabeth Weiland from Siemens Healthcare for providing Metabolite Report.

Research grant: This work was supported by grant number 243115 from the European Research Council under the European Community's Seventh Framework Programme (FP7/2007-2013). The work was partially supported by the intramural research programs of the NIMH and NINDS, NIH.

Abbreviations

ATP	adenosine triphosphate
B_0	magnetic field
B_1^+	transmit radiofrequency amplitude
CoV	coefficient of variation
CRLB	Cramér-Rao lower bound
$\bar{d}$	mean bias between native and NOE-enhanced measurements
η	NOE enhancement

GPC	glycerophosphocholine
GPE	glycerophosphoethanolamine
LoA	limits of agreement
NAD	nicotinamide adenine dinucleotide
$\overline{native}_{repeat}$	mean integral of non-enhanced repeated measurements per voxel
NOE	nuclear Overhauser effect
$\overline{NOEenh}_{repeat}$	mean integral of NOE-enhanced repeated measurements per voxel
MRSI	magnetic resonance spectroscopic imaging
μ	mean metabolite integral over all voxels and measurements
PC	phosphocholine
PCr	phosphocreatine
PE	phosphoethanolamine
Pi	inorganic phosphate
RC	repeatability coefficient
RF	radiofrequency
SAR	specific absorption rate
σ_d	standard deviation of differences between methods
σ_{repeat}	standard deviation of repeated measurements
SNR	signal-to-noise ratio
WALTZ	wideband alternating-phase low-power technique for zero residual splitting

References

1. Solga SF, Horska A, Clark JM, Diehl AM. Hepatic 31P magnetic resonance spectroscopy: a hepatologist's user guide. Liver Int. 2005; 25:490–500. [PubMed: 15910484]
2. Ter Voert EGW, Heijmen L, van Laarhoven HWM, Heerschap A. In vivo magnetic resonance spectroscopy of liver tumors and metastases. World J. Gastroenterol. 2011; 17:5133–5149. [PubMed: 22215937]
3. Argov Z, Löfberg M, Arnold DL. Insights into muscle diseases gained by phosphorus magnetic resonance spectroscopy. Muscle Nerve. 2000; 23:1316–1334. [PubMed: 10951434]
4. Kemp GJ, Meyerspeer M, Moser E. Absolute quantification of phosphorus metabolite concentrations in human muscle in vivo by 31P MRS: a quantitative review. NMR Biomed. 2007; 20:555–565. [PubMed: 17628042]
5. Hudsmith LE, Neubauer S. Magnetic resonance spectroscopy in myocardial disease. JACC Cardiovasc. Imaging. 2009; 2:87–96. [PubMed: 19356540]
6. Martin WRW. MR spectroscopy in neurodegenerative disease. Mol. Imaging Biol. 2007; 9:196–203. [PubMed: 17279431]
7. Andrade CS, Otaduy MCG, Park EJ, Leite CC. Phosphorus-31 MR Spectroscopy of the Human Brain: Technical Aspects and Biomedical Applications. Int. J. Curr. Res. Rev. 2014; 6:41–57.

8. Lagemaat MW, Vos EK, Maas MC, Bitz AK, Orzada S, van Uden MJ, Kobus T, Heerschap A, Scheenen TWJ. Phosphorus magnetic resonance spectroscopic imaging at 7 T in patients with prostate cancer. Invest. Radiol. 2014; 49:363–372. [PubMed: 24335715]
9. Sohlberg S, Wikström A-K, Olovsson M, Lindgren P, Axelsson O, Mulic-Lutvica A, Weis J, Wikström J. In vivo 31P-MR spectroscopy in normal pregnancy, early and late preeclampsia: A study of placental metabolism. Placenta. 2014; 35:318–323. [PubMed: 24612844]
10. Stehouwer BL, van der Kemp WJM, Luijten PR, van den Bosch MAAJ, Veldhuis WB, Wijnen JP, Klomp DWJ. 31P magnetic resonance spectroscopy of the breast and the influence of the menstrual cycle. Breast Cancer Res. Treat. 2014; 144:583–589. [PubMed: 24570008]
11. Luyten PR, Bruntink G, Sloff FM, Vermeulen JW, van der Heijden JI, den Hollander JA, Heerschap A. Broadband proton decoupling in human 31P NMR spectroscopy. NMR Biomed. 1989; 1:177–183. [PubMed: 2641284]
12. Bachert-Baumann P, Ermark F, Zabel H-J, Sauter R, Semmler W, Lorenz WJ. In vivo nuclear overhauser effect in 31P- 1H double-resonance experiments in a 1.5-source whole-body MR system. Magn. Reson. Med. 1990; 15:165–172. [PubMed: 2165209]
13. Freeman DM, Hurd R. Decoupling: theory and practice II. Sate of the art: in vivo applications of decoupling. NMR Biomed. 1997; 10:381–393. [PubMed: 9542736]
14. Brown TR, Stoyanova R, Greenberg T, Srinivasan R, Murphy-Boesch J. NOE Enhancements and T1 Relaxation Times of Phosphorylated Metabolites in Human Calf Muscle at 1.5 Tesla. Magn. Reson. Med. 1995; 33:417–421. [PubMed: 7760710]
15. Mathur-De Vré R, Maerschalk C, Delporte C. Spin-lattice relaxation times and nuclear Overhauser enhancement effect for 31P metabolites in model solutions at two frequencies: implications for in vivo spectroscopy. Magn. Reson. Imaging. 1990; 8:691–698. [PubMed: 2266794]
16. Bottomley PA, Hardy CJ. Proton Overhauser enhancements in human cardiac phosphorus NMR spectroscopy at 1.5 T. Magn. Reson. Med. 1992; 24:384–390. [PubMed: 1569877]
17. Murphy-Boesch J, Stoyanova R, Srinivasan R, Willard T, Vigneron D, Nelson S, Taylor JS, Brown TR. Proton-decoupled 31P chemical shift imaging of the human brain in normal volunteers. NMR Biomed. 1993; 6:173–180. [PubMed: 8394101]
18. Li CW, Negendank WG, Murphy-Boesch J, Padavic-Shaller K, Brown TR. Molar Quantitation of Hepatic Metabolites In Vivo in Proton-decoupled, Nuclear Overhauser Effect Enhanced 31P NMR Spectra Localized by Three-dimensional Chemical Shift Imaging. NMR Biomed. 1996; 9:141–155. [PubMed: 9015801]
19. Lei H, Zhu XH, Zhang XL, Ugurbil K, Chen W. In vivo 31P magnetic resonance spectroscopy of human brain at 7 T: an initial experience. Magn. Reson. Med. 2003; 49:199–205. [PubMed: 12541238]
20. Tyler DJ, Emmanuel Y, Cochlin LE, Hudsmith LE, Holloway CJ, Neubauer S, Clarke K, Robson MD. Reproducibility of 31P cardiac magnetic resonance spectroscopy at 3 T. NMR Biomed. 2009; 22:405–413. [PubMed: 19023865]
21. Wylezinska M, Cobbold JFL, Fitzpatrick J, McPhail MJW, Crossey MME, Thomas HC, Hajnal JV, Vennart W, Cox IJ, Taylor-Robinson SD. A comparison of single-voxel clinical in vivo hepatic 31P MR spectra acquired at 1.5 and 3.0 Tesla in health and diseased states. NMR Biomed. 2011; 24:231–237. [PubMed: 20949641]
22. Lagemaat MW, Maas MC, Vos EK, Bitz AK, Orzada S, Weiland E, van Uden MJ, Kobus T, Heerschap A, Scheenen TWJ. 31P MR spectroscopic imaging of the human prostate at 7 T: T1 relaxation times, Nuclear Overhauser Effect, and spectral characterization. Magn. Reson. Med. 2014; 73:909–920. [PubMed: 24677408]
23. Bland JM, Altman DG. Measuring agreement in method comparison studies. Stat. Methods Med. Res. 1999; 8:135–160. [PubMed: 10501650]
24. Van de Bank, B.; Orzada, S.; Lagemaat, MW.; Bitz, AK.; Scheenen, TWJ. Proceedings of the 22st Annual Meeting of ISMRM. Milan, Italy: 2014. 31P Birdcage Insert for an 8-Channel, Multi-Transmit, 1H Coil at 7T; p. 4810
25. Orzada, S.; Kraff, O.; Schäfer, LC.; Brote, I.; Bahr, A.; Bolz, T.; Maderwald, S.; Ladd, ME.; Bitz, AK. Proceedings of the 17th Annual Meeting of ISMRM. Honolulu, Hawaii, USA: 2009. 8-

Channel Transmit/receive Head Coil for 7 T Human Imaging Using Intrinsically Decoupled Strip Line Elements with Meanders; p. 2999

26. Bitz, AK.; Brote, I.; Orzada, S.; Kraff, O.; Maderwald, S.; Quick, HH.; Yazdanbakhsh, P.; Solbach, K.; Bahr, A.; Bolz, T.; Wicklow, K.; Schmitt, F.; Ladd, ME. Proceedings of the 17th Annual Meeting of ISMRM. Honolulu, Hawaii, USA: 2009. An 8-channel add-on RF shimming system for whole-body 7 Tesla MRI including real-time SAR monitoring; p. 4767
27. Kobus T, Bitz AK, van Uden MJ, Lagemaat MW, Rothgang E, Orzada S, Heerschap A, Scheenen TWJ. In vivo 31P MR spectroscopic imaging of the human prostate at 7 T: Safety and feasibility. Magn. Reson. Med. 2012; 68:1683–1695. [PubMed: 22368094]
28. Shaka A, Keeler J, Freeman R. Evaluation of a new broadband decoupling sequence: WALTZ-16. J. Magn. Reson. 1969. 1983; 53:313–340.
29. Fautz, HP.; Vogel, MW.; Gross, P.; Kerr, AB.; Zhu, Y. Proceedings of the 16th Annual Meeting of ISMRM. Toronto, Ontario, Canada: 2008. B1 mapping of coil arrays for parallel transmission; p. 1247
30. Scheenen TWJ, Klomp DWJ, Röll SA, Fütterer JJ, Barentsz JO, Heerschap A. Fast acquisition-weighted three-dimensional proton MR spectroscopic imaging of the human prostate. Magn. Reson. Med. 2004; 52:80–88. [PubMed: 15236370]
31. Bartlett JW, Frost C. Reliability, repeatability and reproducibility: analysis of measurement errors in continuous variables. Ultrasound Obstet. Gynecol. 2008; 31:466–475. [PubMed: 18306169]
32. Vikhoff-Baaz B, Starck G, Ljungberg M, Lagerstrand K, Forssell-Aronsson E, Ekholm S. Effects of k-space filtering and image interpolation on image fidelity in 1H MRSI. Magn. Reson. Imaging. 2001; 19:1227–1234. [PubMed: 11755733]
33. Cloos MA, Boulant N, Luong M, Ferrand G, Giacomini E, Le Bihan D, Amadon A. kT -points: short three-dimensional tailored RF pulses for flip-angle homogenization over an extended volume. Magn. Reson. Med. 2012; 67:72–80. [PubMed: 21590724]
34. Remy C, Albrand JP, Benabid AL, Decorps M, Jacrot M, Riondel J, Foray MF. In vivo 31P nuclear magnetic resonance studies of T1 and T2 relaxation times in rat brain and in rat brain tumors implanted to nude mice. Magn. Reson. Med. 1987; 4:144–152. [PubMed: 3561243]
35. Edwards LM, Tyler DJ, Kemp GJ, Dwyer RM, Johnson A, Holloway CJ, Nevill AM, Clarke K. The reproducibility of 31-phosphorus MRS measures of muscle energetics at 3 Tesla in trained men. PloS One. 2012; 7:e37237. [PubMed: 22701564]

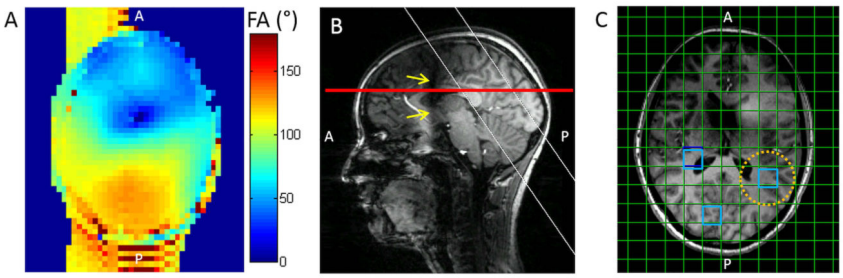

Figure 1.

Overview of preparation steps for native and NOE-enhanced ^{31}P MRSI and data analysis in one subject. A: Transversal absolute ^{1}H B_1^+ map after B_1^+ calibration to obtain at least 90° flip angles in the posterior part of the brain, allowing minimally 30 Hz NOE power. B: Sagittal MPRAGE image. The location of the absolute ^{1}H B_1^+ map is indicated by the red line and the slice selection for flip angle calibration of ^{31}P is indicated by the white lines. The yellow arrows indicate signal dropout due to low B_1^+. C: Transversal MPRAGE images with the spectroscopic grid as an overlay. The voxels indicated in blue were used for data analysis. The approximate real voxel size is indicated by the yellow dotted circle.

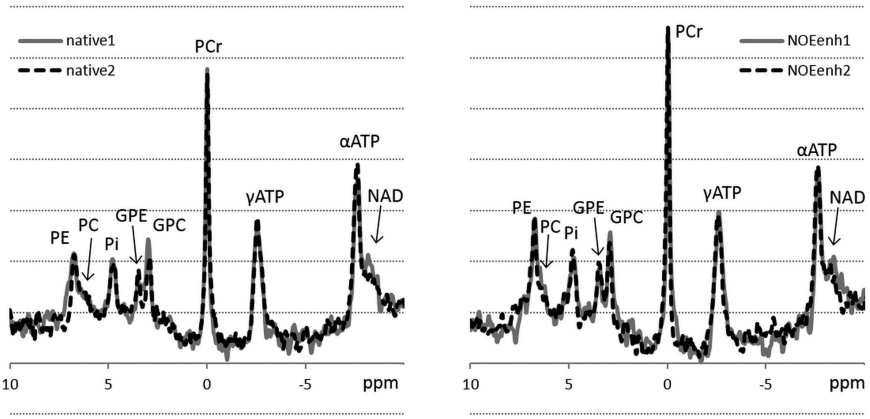

Figure 2.

Example of repeated spectra of the same voxel in one volunteer using native ^{31}P MRSI (left, native) and using NOE-enhanced ^{31}P MRSI (right, NOEenh). Variations between the individual measurements per method are visible, and the NOE-enhanced spectra show a clear increase in signal for several metabolites. PE: phosphoethanolamine, PC: phosphocholine, Pi: inorganic phosphate, GPE: glycerophosphoethanolamine, GPC: glycerophosphocholine, PCr: phosphocreatine, γ- and α-ATP: γ- and α-adenosine triphosphate, NAD: nicotinamide adenine dinucleotide.

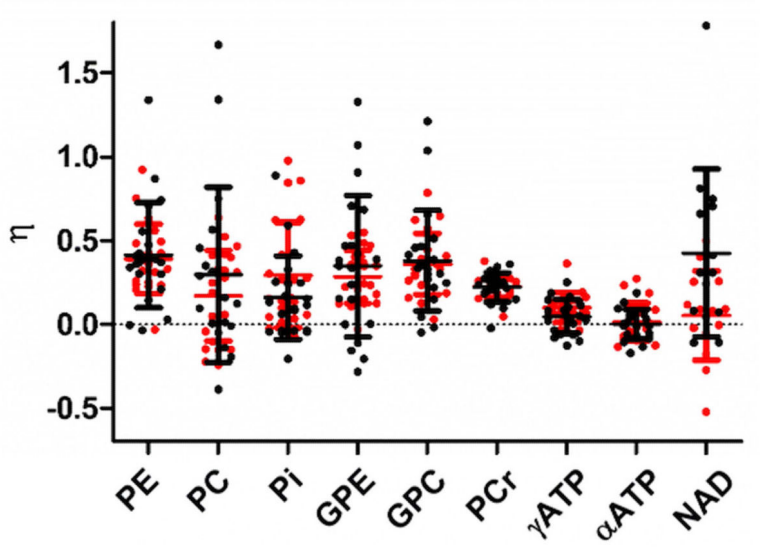

Figure 3.

Nuclear Overhauser Effect (NOE) enhancements (η) per voxel of ^{31}P metabolite resonances in human brain at 7 T. NOE enhancement resulting from the first and second set of native and NOE-enhanced measurements are shown in black and red, respectively.

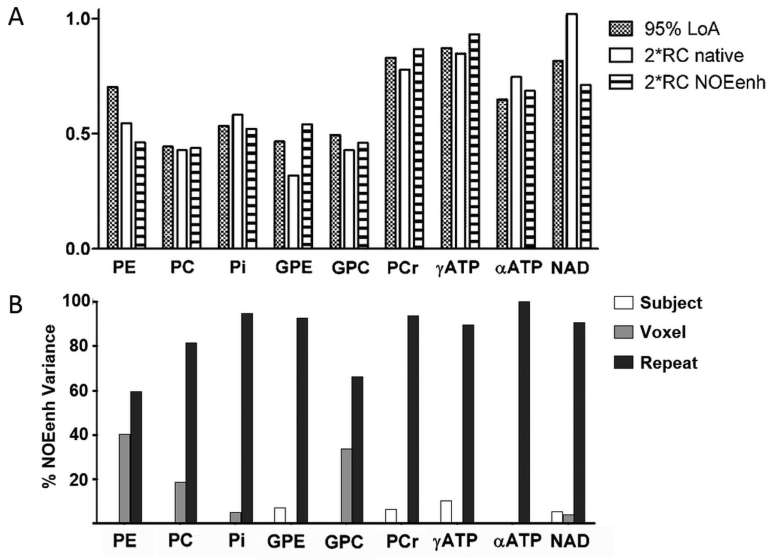

Figure 4.

A: 95% Limits of agreement (LoA) between the two methods and repeatability intervals (2*RC) of each method. B: Variance components in NOE enhancement.

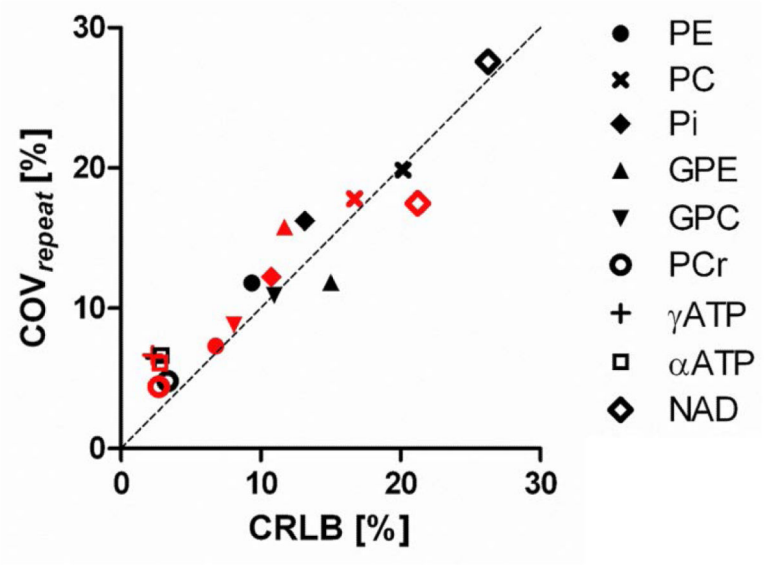

Figure 5.

Relation between fitting error of the metabolites (expressed in percentage Crémer-Rao Lower Bound, CRLB, average across subjects) and the relative repeatability (expressed in the coefficient of variation in repeated measurements, COV_{repeat}) of the metabolites. Black symbols: native. Red symbols: NOE-enhanced.

Table 1

NOE enhancements (±, mean ± SD) and quality of the spectral fit expressed in percentage Cramér-Rao Lower Bounds (CRLB, mean ± SD) of native and NOE-enhanced spectra.

	PE	PC	Pi	GPE	GPC	PCr	γATP	αATP	NAD
η	0.39±0.22	0.19±0.31	0.21±0.20	0.30±0.22	0.36±0.20	0.22±0.05	0.07±0.07	0.00±0.05	0.21±0.23
CRLB native	9.4±1.7	20.2±5.8	13.2±2.6	15.0±3.4	11.0±2.7	3.3±0.8	2.4±0.4	2.9±0.7	26.5±7.4
CRLB NOEenh	6.8±1.0	16.7±4.1	10.8±1.8	11.7±2.6	8.1±1.8	2.7±0.6	2.3±0.3	2.8±0.7	21.2±5.5
p-value	<0.001	0.001	<0.001	<0.001	<0.001	<0.001	0.001	0.56	<0.001

Table 2

Coefficients of Variation in repeated measurement (CoV_{repeat}) of native and NOE-enhanced data per metabolite and for metabolite ratios, as well as the apparent CoV_{repeat} of NOE-enhanced metabolite intensities corrected for their enhancement.

	CoV_{repeat}					
	Native	**NOEenh**	**Corrected**		**Native**	**NOEenh**
PE	11,8%	7,3%	17.4%	**PE/PC**	23,1%	19,3%
PC	19,9%	17,8%	31.6%	**GPE/GPC**	16,1%	18,1%
Pi	16,2%	12,2%	20.6%	**PE/PCr**	12,8%	8,5%
GPE	11,9%	15,8%	23.3%	**Pi/PCr**	16,9%	13,0%
GPC	10,9%	8,8%	17.0%	**(PE+PC)/PCr**	23,2%	17,0%
PCr	4,8%	4,4%	6.2%	**PCr/ γATP**	8,1%	8,0%
γATP	6,5%	6,7%	9.5%	**NAD/ αATP**	28,4%	18,5%
αATP	6,6%	6,1%	7.8%			
NAD	27,6%	17,5%	25.7%			